Centrifugal extraction of plasma from whole blood on a rotating disk

Stefan Haeberle,*[a] Thilo Brenner,[a] Roland Zengerle[ab] and Jens Ducrée[ab]

Received 21st March 2006, Accepted 30th March 2006
First published as an Advance Article on the web 13th April 2006
DOI: 10.1039/b604145k

We present a centrifugal process for the extraction of plasma from sediment by a decanting structure, terminating with metered plasma which is readily available for subsequent on-disk processing. Our technique supplies 2 μl plasma from 5 μl of whole blood at moderate spinning frequencies of 40 Hz within 20 s, only. The residual cell concentration in the purified plasma amounts to less than 0.11%, independent of the frequency of rotation. A capillary duct connects the extracted plasma to subsequent on-disk processing units.

1. Introduction

The transfer of clinical diagnostics from centralized laboratories to the point of care/point of use is the focus of intensive research and development over the last decade. An important aspect is the comprehensive integration of all protocol steps from the preparation of whole blood to the analytical result. Associated benefits are reduced turn-around times, improved control over critical process parameters due to automation, elimination of labor intensive steps and reduced consumption of precious sample and reagents. The techniques required for sample preparation and detection are addressed by so-called "lab-on-a-chip" technologies.[1–6] The high potential of these systems already epitomizes a considerable number of commercially available diagnostic devices.[7]

The extraction of plasma from whole blood is the first preparative step in many assay protocols and of major importance in medical diagnostics. The quality of the separation process is determined by the purity of the plasma, the separation time, the yield of extracted plasma from the whole blood sample and by the suppression of hemolysis. In addition, the separation process must allow a seamless integration with subsequent assay steps to avoid manual intervention or expensive interconnection techniques.

Centrifugal microfluidic platforms[8–11] are of particular interest for assay integration as their artificial gravity field intrinsically implements a pumping force as well as an established method for particle separation without actuation apart from a standard rotary drive. While several microfluidic approaches for sample preparation and detection such as cell lysis,[12] batch-mode mixing,[13] protein assays[14,15] and sample preparation for MALDI-MS[16] have been presented so far, a robust and integrable structure for plasma extraction[17] is essential for a complete on-disk processing. We present here a novel decanting process for the extraction of plasma from the cellular constituents, terminating with metered plasma which is readily available for subsequent on-disk processing.

This paper is structured in the following way. Section 2 compiles the basic laws governing a centrifugal separation process. Section 3 introduces the here implemented flow scheme of our decanting process, *i.e.*, the separation of a metered plasma volume. Section 4 summarizes the fabrication process of the microfluidic structure which is experimentally investigated in Sections 5 and 6. Before concluding, we portray how the extracted plasma can be forwarded to a subsequent structure in Section 7 to realize complex tasks on the centrifugal platform.

2. Physics of centrifugal sedimentation

Phase separation in a centrifugal field caused by a difference in mass density is called sedimentation. Compared to natural gravity, the sedimentation of suspended particles in centrifugal fields can be extensively accelerated since the centrifugal net force

$$F_v = (2\ \pi\ v)^2\ z_p\ V_p(\rho_p - \rho_l) \quad (1)$$

induced on a particle of volume V_p at radial position z_p scales with the square of rotational frequency v. Particles of mass densities ρ_p falling short of the liquid mass density ρ_l are driven radially inwards whereas denser particles settle outwards.

When the particle with radius r_p drifts in liquid medium of viscosity η at velocity u_d (under laminar conditions), the friction force

$$F_S = -6\ \pi\ \eta_l\ r_p\ u_d \quad (2)$$

caused by the Stokes drag counteracts the centrifugal force F_v.

The equation of centrifugal force (1) and friction (2) leads to the constant drift velocity of the particle

$$u_{drift} = s_p\ z_p\ (2\ \pi\ v)^2 \quad (3)$$

at steady state. The particle sedimentation coefficient s_p is defined as

$$s_p = \frac{m_p}{6\pi\eta_l r_p}\left(1 - \frac{\rho_l}{\rho_p}\right) \quad (4)$$

[a]*Laboratory for MEMS Applications, Department of Microsystems Engineering (IMTEK), University of Freiburg, Georges-Koehler-Allee 106, D-79110 Freiburg, Germany*
[b]*HSG-IMIT – Institute of Micromachining and Information Technology, Wilhelm-Schickard-Straße 10, D-78052 Villingen-Schwenningen, Germany. E-mail: haeberle@imtek.de; Fax: +49 761 203 7539; Tel: +49 761 203 7476*

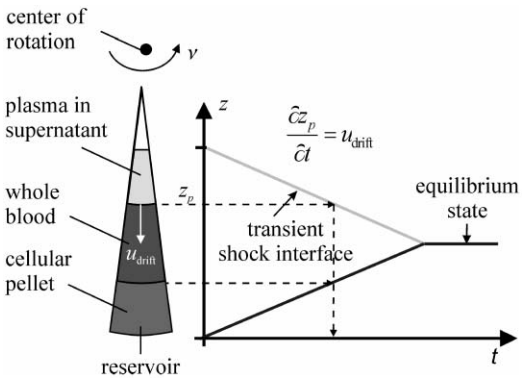

Fig. 1 Intermediate state of batch mode sedimentation in a centrifugal field. A *shock interface* proceeds at a velocity u_{drift}. Eventually, red blood cells are concentrated in a pellet on the bottom of the vessel while purified plasma is found in the supernatant.

with particle mass m_p. The sedimentation coefficient for red blood cells is empirically determined to 0.27×10^{-7} s.[18]

The course of a conventional sedimentation in a centrifugal field is depicted in Fig. 1. The red blood cells (RBCs) which possess a larger mass density than the plasma are driven by the centrifugal field towards the bottom of the reservoir. During the separation, a sharp interface forms between the already purified plasma without cells, and the subjacent cell suspension.

This interface is also referred to as *shock-interface* since it represents an abrupt discontinuity in the cell concentration of the suspension. At the end of the separation, a radial stack constituted by a cellular pellet at the bottom and a purified plasma supernatant evolves. The reader may notice that the constant propagating of the *shock interface* at speed u_{drift} is a simple model disregarding the hindered settling effect [19] which results in a decreasing u_{drift} with increasing particle concentration towards the end of the separation. Since the cells are not concentrated up to such a critical concentration in our proposed decanting technique, the simple model is sufficient to describe the principle of our structure.

3. Centrifugal flow scheme

The plasma in the supernatant has to be separated from the cellular pellet. In contrast to manual extraction by a pipette after centrifugation, a fully integrated, multi-step sample processing affords an on-disk extraction. In our concept, we split the two phases during sedimentation by a decanting process (Fig. 2) which is explained in the following.

The device comprises a metering structure which is connected *via* a drain channel to two subsequent chambers, a first chamber to sediment and retain the cells followed by another reservoir receiving the purified plasma through a decanting mechanism. In the presented design, the drain channel is located at a radius of 32 mm on the rotating disk exhibiting an overall diameter of 120 mm (corresponding to the format of a conventional compact disc).

Initially, a raw blood sample is metered to a fixed volume defined by an overflow channel next to the inlet and a hydrophobic stop at the outlet of the metering chamber.

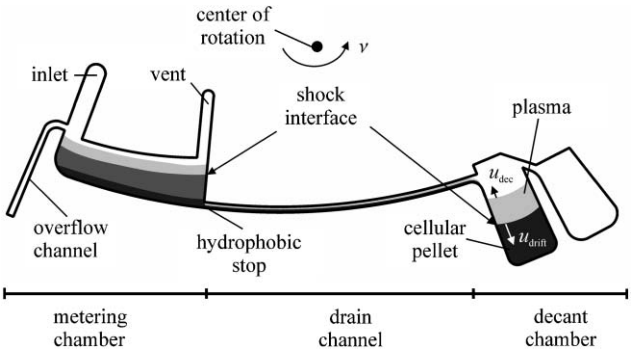

Fig. 2 Flow scheme in our separation structure. A metered volume of the blood sample defined between hydrophobic stop and overflow channel flows from the metering chamber *via* the drain channel into the decant structure. A shock interface separating plasma from the cellular pellet builds out in all parts of the network and proceeds radially outwards at a speed u_{drift}. The filling height of the decant chamber rises at counter-current speed u_{dec} before the plasma overflows into the plasma collection chamber. The speed u_{dec} of the filling height in the cell reservoir is adjusted by the hydrodynamic resistance of the drain channel so that only purified plasma advances to the plasma reservoir.

Subsequently, the metered sample is forwarded *via* the drain channel to the decanting structure.

The volume flow of blood from the metering chamber through the drain channel

$$I_V(v,t) = \frac{p_v(v,t)}{R_{hd}} \sim v^2 \tag{5}$$

is determined by the quotient of the (equivalent) centrifugal pressure p_v (v, t) and the flow resistance R_{hd} of the channel network. This centrifugal pressure[20]

$$p_v(v,t) = \rho_b (2\pi v)^2 \bar{r}_b(t) l_b(t) \sim v^2 \tag{6}$$

scales with the square of rotational frequency v, the mass density ρ_b of the blood sample, the radial length l_b of the liquid column and the medium radial position r_b which both change over time t during the decanting process.

The flow resistance

$$R_{hd} = C_{nc} \frac{\eta_b l_{drain}}{\rho_b A_{drain}^2} \tag{7}$$

is dominated by the cross section A_{drain} and the length l_{drain} of the drain channel in addition to viscosity η_b and mass density ρ_b of the whole blood. C_{nc} is a geometry-dependent coefficient.[21] The cross-sections of the reservoirs are very large compared to the cross-section of the long drain channel and can hence be discarded in R_{hd}.

During decanting, the suspended red blood cells sediment in the centrifugal field at the velocity u_{drift} and a shock interface emerges in all parts of the network which are already primed with blood. When the cell reservoir is entirely filled, plasma in the supernatant overflows into the plasma chamber.

Two conditions have to be satisfied in order to ensure that only purified plasma in the supernatant overflows into the subsequent plasma reservoir: First, the volume capacity of the cell chamber must exceed the volume fraction of cells.

Secondly, the ratio between the speeds of the filling level u_{dec} and the opposing speed of the shock interface u_{drift} must remain small enough such that the cellular constituents never proceed to the plasma chamber. This is, for instance, guaranteed for $u_{dec} < u_{drift}$ during the later stages of the sedimentation process.

The speed of the filling level in the cell reservoir

$$u_{dec}(v,t) = \frac{I_V}{A_{cell}} = \frac{p_v(v,t)}{A_{cell} R_{hd}} \sim v^2 \quad (8)$$

is given by the volume flow I_V out of the drain channel and the cross-sectional area A_{cell} of the cell chamber.

As both, u_{dec} (8) as well as u_{drift} (3), scale with the square of the spinning frequency v, the ratio of the two velocities turns out to be constant over v, thus making the basic working principle of our sedimentation structure independent of v. Furthermore, the volume efficiency, *i.e.*, the ratio of the extracted plasma to the initially metered volume of whole blood, coincides with volume defined by the metering on the inlet side and the volume capacity of the sedimentation chamber.

The course of separation concludes when the entire blood sample is decanted from the metering chamber into both decant chambers.

4. Fabrication

The channels and reservoirs are fabricated by photopatterning multilayers of thick photoresist SU-8[22] which are then replicated into disks of cyclo-olefin copolymer (COC) by soft embossing.[23] Therefore, the SU-8 structure is cast into an elastomer (PDMS) which acts as the tool in the hot embossing process. Afterwards, the structured polymer disk as well as the lid are globally hydrophilized by plasma activation (O_2–plasma of 100 W for 1 min). Hydrophobic patches are subsequently applied using a 1% Teflon solution on designated channel sections.

In order to avoid a sagging of the cover-lid, a 2-composite polymer foil featuring two layers is used in the thermal diffusion bonding process. One 0.5 mm stiff layer supplies the required mechanical stability to the lid while a only 3 to 5 μm thick second layer promotes the bonding due to its low glass transition temperature. The channel width amounts to 300 μm and the depth is measured to 85 μm; the depths of the reservoirs are 300 μm.

5. Experimental investigation

The blood samples for all presented experiments were pretreated with the anticoagulant EDTA. Also separations with pure human whole blood obtained from the finger tip with a commercial lancet system could be successfully performed. The Hematocrit (volume fraction of red blood cells) has not been measured or adjusted and thus varied within the typical physiological range (42% to 52% for males and 36% to 48% for women). However, since the quality of separation in terms of the purity and the volume of the extracted plasma remained constant on different days for a variety of test persons, the method proved to be highly reproducible and robust with respect to varying properties of the blood sample.

The blood is injected into the channel network, primes the metering chamber and the overflow channel by capillary action and stops at the hydrophobic patch. The centrifugal separation protocol comprises two operational frequencies. In the first metering step (Fig. 3, left), the disk spins at a low frequency of 10 Hz which is smaller than the burst frequency (15 Hz) of the hydrophobic valve at the outlet of the metering chamber. The liquid plug within the inlet and overflow channel drains into the waste reservoir and tears off from the liquid volume of 5 μl defined by the chamber geometry.

Leakage of metered sample into the overflow channel is suppressed by tailoring a tiny meniscus at the inlet of the metering chamber. This way, the impact of uncontrollable fluctuations of the break-off process on the much larger volume to be metered are minimized. The break-off is thus enforced by a sharp constriction (“liquid knife”) at the transition from the metering chamber to the overflow channel. In addition, the entrance region of the overflow channel is widened to locally weaken the impact of the capillary force and

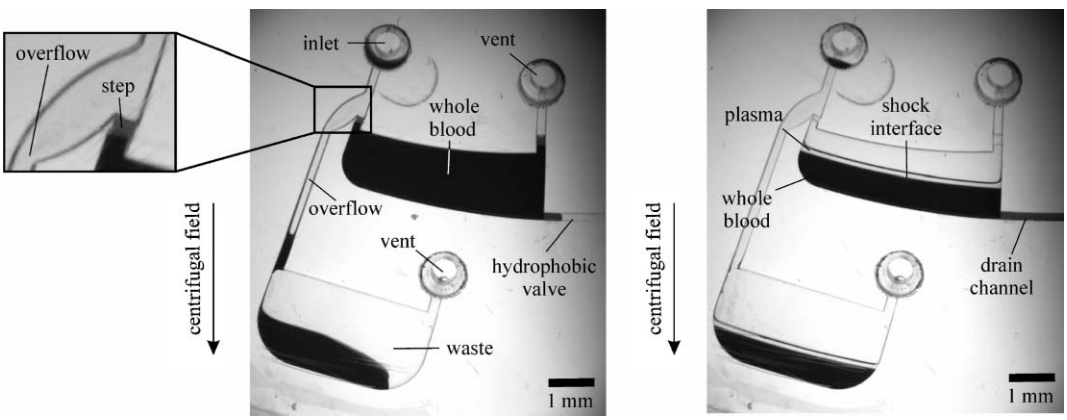

Fig. 3 (Left) In the metering chamber, whole blood is centrifugally metered to a volume of 5 μl at rotational frequency v = 10 Hz. The volume is defined between the hydrophobic stop at the outlet and the overflow channel next to the inlet of the chamber. The vent ensures optimum capillary filling. (Right) At v = 40 Hz, blood flows out of the metering chamber into the drain channel at flow rate I_v (v,t). The evolution of the shock interface between plasma and cellular blood constituents can be observed.

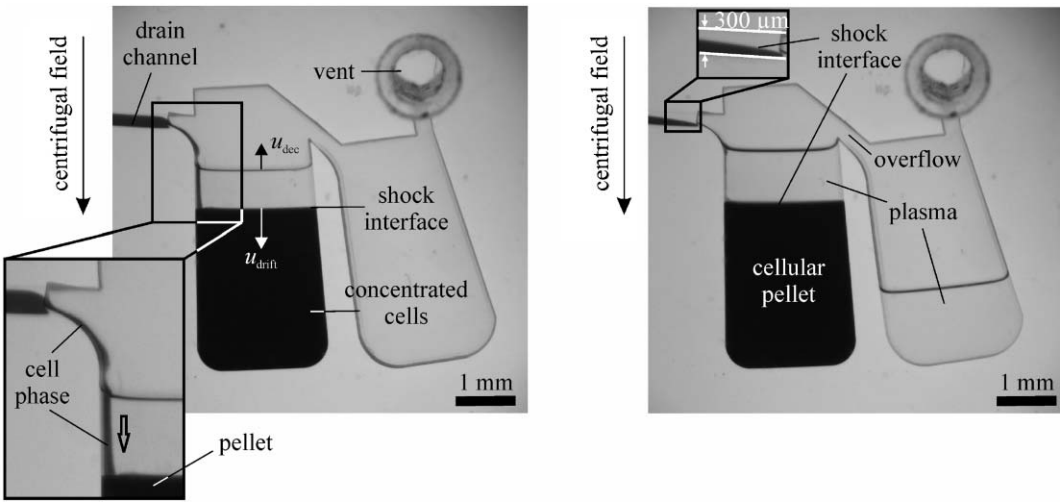

Fig. 4 (Left) Intermediate state of the decanting process at v = 40 Hz. Blood from the drain channel flows into the first reservoir. The filling level moves at a speed u_{dec} (v,t) towards the radially inwards overflow while the shock interface separating pure plasma in the supernatant from the cellular pellet progresses radially outwards. (Right) Advanced state of separation. Purified plasma is decanted into a separate reservoir while the cellular pellet is retained at the bottom of the decant chamber. The shock interface separating plasma and cellular sediment in the drain channel is magnified in the insert.

thus "pin" the emerging liquid/gas interface at a well-reproducible position.

At frequencies beyond the burst frequency of 15 Hz (here 40 Hz), the decanting procedure initiates through the drain channel into the decant chambers (Fig. 3, right). During filling of the first decant chamber, the radially outwards moving shock interface separates plasma and cellular sediment (Fig. 4, left). The flow resistance of the drain channel throttles the filling so that only plasma in the supernatant overflows into the second chamber (Fig. 4, right). The process yields 2 µl of purified plasma in the final reservoir where it is readily available for further on-disk processing. The images are acquired by a stroboscopic technique.[24]

In addition to the "conventional" separation in the decant chamber, also the continuous pre-separation in the narrow drain channel contributes to the enhanced speed and quality of the plasma extraction process. Due to the small radial extension (300 µm) of the drain channel, a 2-phase flow emerges shortly after exiting the metering chamber (see magnified excerpt on the right of Fig. 4). Once the stacked flow reaches the entrance of the decant chamber, it can be observed that the lower cell phase directly proceeds along the left wall of the separation chamber to the high-density pellet at the bottom while the less dense upper plasma phase immerses with the supernatant (Fig. 4, left). The pre-separation in the drain channel thus remains widely undisturbed by the transition from the flow through the drain channel to the batch-mode separation chamber.

Also the confinement of the inflowing cells to the left hand side favors a clean separation from the plasma overflow on the opposite side of the separation chamber. We also mention that, as the pre-separated plasma "slips" more rapidly through the upper part of the drain channel, the cell concentration and thus the viscosity of the suspension tends to increase to steadily reduce the flow velocity through the drain channel.

The separation of the 5 µl volume takes place at high frequencies to reduce the time t_{sep} for gaining the targeted plasma volume of 2 µl. Fig. 5 shows the measured separation time t_{sep} for different rotational frequencies from 25 Hz to 50 Hz. Our experiments corroborate a decline of the separation time t_{sep} with inverse square of the frequency v which complies with the theory (5). However, a minimum separation time is imposed by the practical limitation of the centrifugal frequency by the power of the rotary engine, the bonding strength of the lid, parasitic hemolysis and general security issues. A reasonable trade-off is found at a spinning frequency of v = 40 Hz.

As already described in Section 3, the shock interface occurs in all parts of the separation structure as soon as the disk starts the high-frequency rotary motion (Fig. 3, right). Thus, the cell concentration of the blood-flow out of the metering chamber is slightly increased within the first stage of the process (higher viscosity of blood), leading to a deceleration of u_{dec} and making the whole process even more stable.

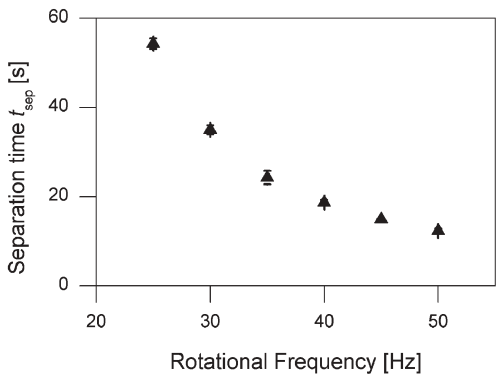

Fig. 5 The measured separation time t_{sep} declines with the inverse square of the spinning frequency v.

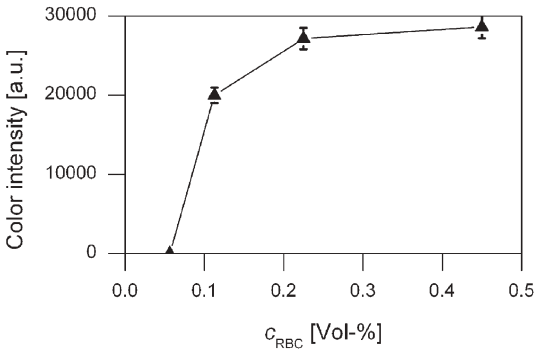

Fig. 6 Calibration curve between color intensity and cell suspension with a defined concentration of red blood cells c_{RBC}. The limit of detection is a concentration c_{RBC} = 0.1125%.

6. Residual cell concentration

The extracted plasma is investigated for residual red blood cells by optical inspection of the bottom of the reservoir and the liquid/gas interface (Fig. 7) for all rotational frequencies ν. Prior to inspection, the disk is again extensively spun at 100 Hz for more than 5 min to ensure that all residual cells in the bulk of the plasma agglomerate at the reservoir bottom. Color images of the reservoir bottom are taken and compared to agglomerated cells of defined concentrations (Fig. 6). With this method, the residual cells in the plasma are determined to less than 0.1125% independent of the rotational frequencies during separation. The true cell concentration is probably even smaller as the limit of 0.1125% corresponds to the minimum detectable cell concentration.

Inspecting the radially inward liquid/gas interface, a thin film of cells on the plasma meniscus can be observed. Presumably stabilized by the surface tension, the few cells stay on top of the liquid and do not penetrate through the surface into the bulk, even by spinning at maximum rotational frequencies of 100 Hz. The purity of the bulk plasma is thus not affected for further on-disk processing, especially when it is capillary sucked away from the bottom of the reservoir (Fig. 8). We assume that residual cells on top of the liquid directly migrate from the drain channel into the plasma chamber on top of the liquid meniscus when the first decant chamber

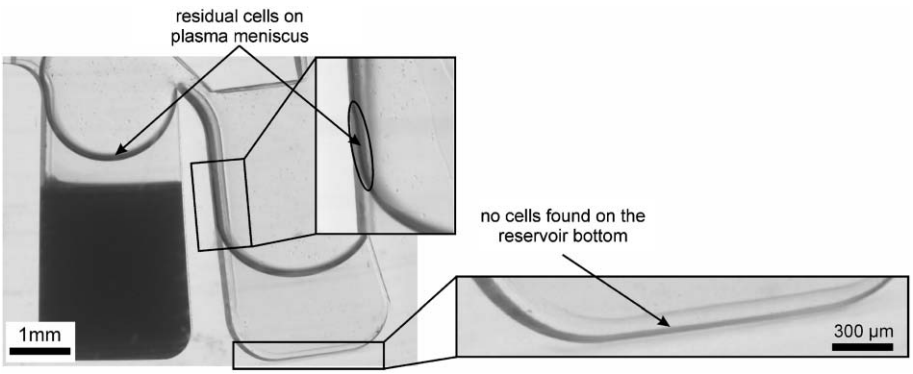

Fig. 7 Two areas are investigated for residual red blood cells after sedimentation: the bottom of the reservoir and the plasma meniscus. Even after extensive centrifugation at 100 Hz for 5 min, no residual cells are found at the bottom of the plasma reservoir according to the minimum detectable cell concentration of 0.1125% (Fig. 6). However, residual cells on top of the plasma meniscus are observed even after the centrifugation in both reservoirs. They do not penetrate the surface of the meniscus and thus do not affect the purity of the bulk plasma.

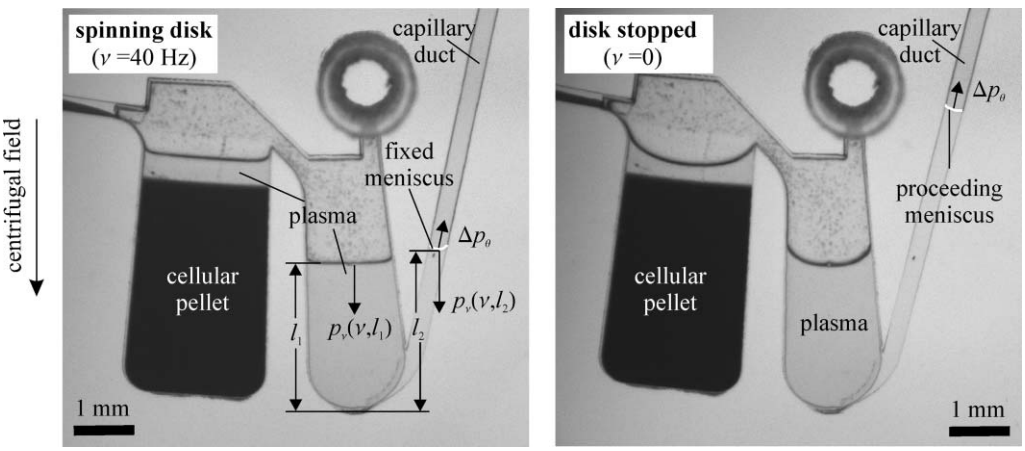

Fig. 8 (Left) A capillary duct connects the bottom of the plasma reservoir to potential subsequent analyses located in the center of the disk. During rotation, the plasma is retained in the plasma reservoir by the high centrifugal pressures $p_\nu(\nu,l)$ in the reservoir (l_1) and the duct (l_2), dominating capillarity. (Right) Upon stopping the disk, the plasma primes the capillary duct by capillary action Δp_θ and proceeds towards the center of the disk for further on-disk processing.

already overflows in the final phase of separation. It should be mentioned as well that no hemolysis was observed by visual inspection of the extracted plasma in all experiments.

7. Capillary forwarding of plasma

In order to allow further on-disk processing, the extracted plasma is capillary forwarded towards the center of the disk by a capillary duct connected to the bottom of the plasma reservoir.[8] During rotation of the disk, the position of the advancing meniscus is governed by the principle of interconnected tubes in the centrifugal field, prevailing the small bias due to the diverging capillary pressures Δp_θ at the confining menisci. This way, the plasma sample is retained in the reservoir (Fig. 8, left). Upon stopping the disk, the plasma in the reservoir is pulled into the duct by the remaining capillary force to drive the meniscus towards the center of the disk for further processing (Fig. 8, right).

Conclusions

Our continuous centrifugal flow separation technique efficiently extracts 2 µl plasma from a raw blood sample that is metered to 5 µl. Typical separation times of 20 s could be achieved for moderate spinning frequencies of 40 Hz. The residual cell concentration in the bulk plasma is smaller than 0.1125% and independent from frequency, showing the robustness of the concept. The microfluidic structure can easily be adapted for an integrated sample processing on centrifugal platforms.

Acknowledgements

This work was supported by grants from "Landesstiftung" of the German federal state of Baden-Württemberg, (Bio-Disk, 24-720, 431-1-7/2).

References

1 A. J. Tudos, G. A. J. Besselink and R. B. M. Schasfoort, *Lab Chip*, 2001, **1**, 2, 83–95.
2 T. Vilkner, D. Janasek and A. Manz, *Anal. Chem.*, 2004, **76**, 3373–3386.
3 D. Reyes, D. Iossifidis, P. Auroux and A. Manz, *Anal. Chem.*, 2002, **74**, 2623–2636.
4 P. Auroux, D. Reyes, D. Iossifidis and A. Manz, *Anal. Chem.*, 2002, **74**, 2637–2652.
5 P. Gravesen, J. Branebjerg and O. S. Jensen, *J. Micromech. Microeng.*, 1993, **3**, 4, 168–182.
6 J. Ducrée and R. Zengerle, *FlowMap—Microfluidics roadmap for the life sciences*, Books on Demand, GmbH: Norderstedt, Germany, ISBN 3-8334-0744-1, 2004, www.microfluidics-roadmap.com, accessed 2005.
7 Examples in clinical diagnostics: Careside Analyzer®, Careside Inc, USA, www.careside.com; Biosite® Biosite Inc., France, www.biosite.com; Pelikan SunTM of Pelikan Technologies Inc., USA, www.pelikantechnologies.com; Chempaq Analyzer, Chempaq A/S, Denmark, www.chempaq.com; i-STAT Portable Clinical Analyzer, i-STAT Corp., USA, www.istat.com; Abaxis Piccolo®, Abaxis Inc., USA, www.abaxis.com; (all URLs accessed 2005).
8 C. T. Schembri, T. L. Burd, A. R. Kopf-Sill, L. R. Shea and B. Braynin, *J. Autom. Chem.*, 1995, **17**, 3, 99–104.
9 M. J. Madou and G. J. Kellogg, *Proc. SPIE-Int. Soc. Opt. Eng.*, 1998, **3259**, 80–93.
10 G. Ekstrand, C. Holquist, A. Örlefors, B. Hellman, A. Larsson and P. Andersson, *Proceedings of Micro Total Analysis Systems*, Kluwer Academic Publisher, Dordrecht, The Netherlands, 2000, pp. 311–314.
11 J. Steigert, M. Grumann, T. Brenner, K. Mittenbühler, T. Nann, J. Rühe, I. Moser, S. Haeberle, L. Riegger, J. Riegler, W. Bessler, R. Zengerle and J. Ducrée, *J. Assoc. Lab. Automation (JALA)*, 2005, **10**, 5, 331–341.
12 J. Kim, S. H. Jang, G. Y. Jia, J. V. Zoval, N. A. Da Silva and M. J. Madou, *Lab Chip*, 2004, **4**, 5, 516–522.
13 M. Grumann, A. Geipel, L. Riegger, R. Zengerle and J. Ducrée, *Lab Chip*, 2004, **5**, 5, 560–565.
14 D. C. Duffy, H. L. Gillis, J. Lin, N. F. Sheppard and G. J. Kellogg, *Anal. Chem.*, 1999, **71**, 20, 4669–4678.
15 G. Thorsén, G. Ekstrand, U. Selditz, S. R. Wallenborg and P. Andersson, *Proceedings of Micro Total Analysis Systems*, MESA Monographs, 2003, pp. 457–460.
16 M. Gustafsson, D. Hirschberg, C. Palmberg, H. Jörnvall and T. Bergman, *Anal. Chem.*, 2004, **76**, 2, 253–502.
17 T. Brenner, S. Haeberle, R. Zengerle and J. Ducrée, *Proceedings of Micro Total Analysis Systems MicroTAS 2004*, Malmö, Sweden, September 26–30, 2004, pp. 566–568.
18 B. J. Van Wie and E. L. Hustvedt, *Biorheology*, 1988, **25**, 651–662.
19 G. J. Kynch, *Trans. Faraday Soc.*, 1952, **48**, 2, 166–176.
20 T. Brenner, T. Glatzel, R. Zengerle and J. Ducrée, *Lab Chip*, 2005, **5**, 2, 146–150.
21 M. Richter, P. Woias and D. Weiss, *Sens. Actuators, A*, 1997, **62**, 1–3, 480–483.
22 H. Lorenz, M. Despont, N. Fahrni, J. Brugger, P. Vettinger and P. Renaud, *Sens. Actuators, A*, 1998, **64**, 1, 33–39.
23 B. L. Carvalho, E. A. Schilling, N. Schmid and G. J. Kellogg, *Proceedings of Micro Total Analysis Systems*, MESA Monographs, 2003, pp. 959–962.
24 M. Grumann, T. Brenner, C. Beer, R. Zengerle and J. Ducrée, *Rev. Sci. Instrum.*, 2005, **76**, 025101.